From Local to Nonlocal High-Q Plasmonic Metasurfaces

Yao Liang,[1] Din Ping Tsai,[1,2,3,*] and Yuri Kivshar[4,†]

[1]*Department of Electrical Engineering, City University of Hong Kong, Kowloon, Hong Kong SAR, China*
[2]*State Key Laboratory of Terahertz and Millimeter Waves, City University of Hong Kong, Kowloon, Hong Kong SAR, China*
[3]*Centre for Biosystems, Neuroscience and Nanotechnology, City University of Hong Kong, Kowloon, Hong Kong SAR, China*
[4]*Nonlinear Physics Center, Research School of Physics, Australian National University,*
Canberra, Australian Capital Territory 2601, Australia

(Received 27 November 2023; revised 26 May 2024; accepted 28 June 2024; published 29 July 2024)

The physics of bound states in the continuum (BICs) allows the design and demonstration of optical resonant structures with large values of the quality factor (Q factor) by employing dielectric structures with low losses. However, BIC is a general wave phenomenon that should be observed in many systems, including the metal-dielectric structures supporting surface plasmon polaritons where optical resonances are hindered by losses. Here we suggest and develop a comprehensive strategy to achieve high-Q resonances in plasmonic metasurfaces by effectively tailoring the resonant modes from local to nonlocal regimes, thus transitioning from quasi-isolated localized resonances to extended resonant modes involving strong interaction among neighboring structure metaunits.

DOI: 10.1103/PhysRevLett.133.053801

Introduction—Recent progress in metaphotonics is driven by the physics of optical resonances allowing us to achieve high values of the radiative quality factor (Q factor). One mechanism enabling high-Q dielectric metaphotonics is based on the physics of bound states in the continuum (BICs), which support sharp resonances for spatially localized modes within the continuum spectrum of extended states [1]. An ideal BIC in metasurfaces [2] is a dark state with an infinite lifetime that in practice always transforms into a quasi-BIC (qBIC) mode with finite Q manifested in the Fano effect. The study of BICs and qBICs has attracted much attention in recent years. The BIC concept has been employed for many problems requiring the enhancement of light-matter interaction with many applications including nanolasers [3,4], harmonic generation [5], biosensing [6], and optical imaging [7].

In a majority of applications, BICs are realized in *dielectric photonic structures* fabricated of materials with high value of refractive index [6–9], and the underlying physics explores the idea to reduce the *radiative Q factor* by adjusting geometric parameters, such as asymmetry of meta-atoms composing metasurfaces [2]. At the same time, several recent studies demonstrated the use of the BIC concept for hybrid metal-dielectric [10–12] and purely plasmonic [13–15] nanostructures.

We notice that the BIC concept relies on the basic principles of wave physics and wave interference [16]; thus, in general, it should be applied to both low-loss dielectric and high-loss plasmonic structures. The main question is, what is the general strategy for engineering high-Q resonances in plasmonic structures? In this Letter, we uncover the basic physics underpinning high-Q plasmonic structures via the manipulation of dissipative properties of the resonant modes during the transition between local and nonlocal regimes in plasmonic metasurfaces. Here, "local" signifies quasi-isolated site resonances characterized by localized E fields and minimal mutual interaction among metaunits, whereas "nonlocal" indicates collective resonances with significantly extended E fields and strong interaction among metaunits.

Local to nonlocal transition in the parameter space—To illustrate our general strategy, first we focus on one recent example of a plasmonic metasurface (Fig. 1), consisting of vertical split-ring resonators (VSRRs) on a golden film substrate [13]. This plasmonic structure supports dark and

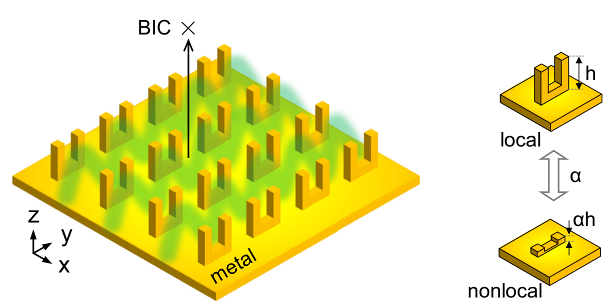

FIG. 1. Left: light trapping in a plasmonic (gold) BIC metasurface with vertical split-ring resonators. Right: transition between local and nonlocal resonances through the parameter scaling, with α being the scaling parameter.

*Contact author: dptsai@cityu.edu.hk
†Contact author: yuri.kivshar@anu.edu.au

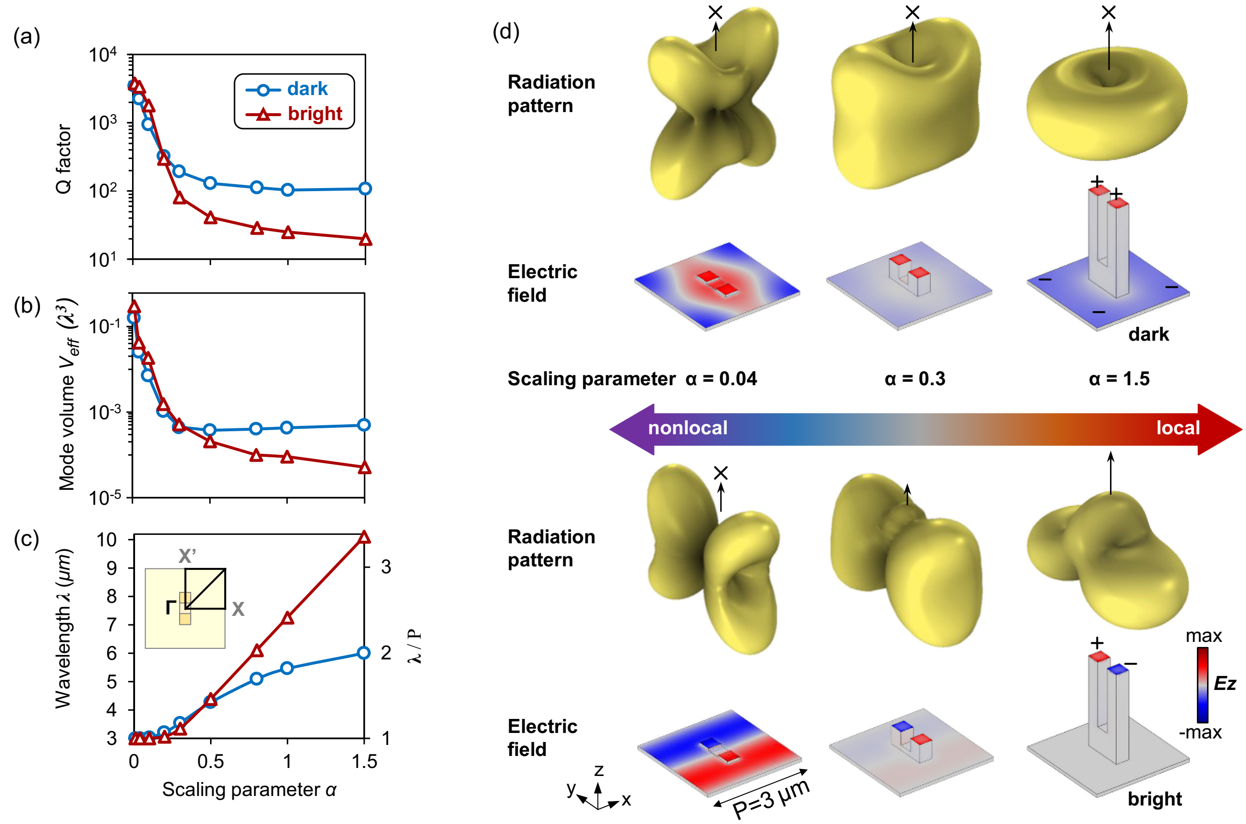

FIG. 2. Eigenmode analysis at the Γ point of VSRR metasurfaces. (a)–(c) The Q factor, mode volume, and resonance wavelength dependence on the scaling parameter α for the dark and bright modes. The initial parameters (at $\alpha = 1$) are period 3 μm, square pillar width 0.4 μm and high 1.8 μm, middle connector height 0.5 μm, center-to-center distance between pillars 0.8 μm. (c) Inset: Γ-point position. (d) The radiation patterns and electric fields ($\boldsymbol{Ez}$) for various α.

bright localized surface plasmon resonances (LSPRs). The initial geometric parameters are shown in the caption of Fig. 2. By exclusively scaling the height parameters (the pillars and middle-connector heights) with the scaling factor α while keeping other parameters constant, it facilitates a transition between local and nonlocal regimes for both the modes. Here, $\alpha > 1$ indicates an increase, while $\alpha < 1$ indicates a decrease.

Figure 2 illustrates this transition in parameter space at the Γ point of arrays, specifically, at the in-plane emission wave vector $k_{\parallel} = (k_x, k_y) = 0$, where k_x and k_y denote the wave vector components along the x and y axes. We categorize odd and even symmetry LSPRs, corresponding to in-plane and out-of-plane resonances, as bright and dark modes based on their far-field radiation at local regimes. Decreasing the scaling parameter α from 1.5 to 0.01 leads to a shift from local to nonlocal resonance with two notable features: (1) the resonance wavelengths (in free space) approach the period ($\lambda \to P$, where $P = 3$ μm), as shown in Fig. 2(c); (2) a significant increase in Q factor [Fig. 2(a)], and mode volume [Fig. 2(b)] for both modes, with differences spanning several orders of magnitude. The Q factor is calculated using $Q = \omega_r / 2\omega_i$, where ω_r and ω_i are the real and imaginary parts of eigenfrequencies.

In pure local regimes, when $\alpha = 1.5$, the bright LSPR mode, for example, exhibits a resonance wavelength ($\lambda \sim 10$ μm) several times larger than the lattice period ($P = 3$ μm), as shown in Fig. 2(c). The individual unit resonance (local) prevails in this local LSPR, overshadowing negligible contributions from collective resonances (nonlocal) that depend on strong interactions among neighboring units [17]. This is evident because a single isolated unit exhibits a nearly identical electric field profile and spectral enhancement as the entire array [see Supplemental Material (SM) [18], S3].

However, the Q factor for the bright LSPR is low, $Q \approx 19.8$ at $\alpha = 1.5$ [Fig. 2(a)]. This is predominantly attributed to two reasons.

First, its tight light confinement, evident through hot spots on the tops of pillars [Fig. 2(d)] and an ultrasmall mode volume (SM [18], S2) well below the diffraction limit [$V_{\mathrm{eff}} \sim 5.13 \times 10^{-5} \lambda^3$, Fig. 2(b)]. These hot spots amplify the electric field ($|\mathbf{E}|$), causing a notable increase in the metal's dissipation density, $w = 1/2\epsilon_0 \mathrm{Im}(\epsilon)|\mathbf{E}|^2$, where ϵ_0 and $\epsilon = \epsilon_r + i\epsilon_i$ denote the vacuum permittivity and relative permittivity of gold. This giant dissipation loss hampers sustaining light energy exchange between the E field and the H field, preventing high-Q resonances. The reason is simple: high-Q resonances, known for long-lasting light oscillation in cavities, require a sustaining oscillation between electric field energy ($u_E \propto \epsilon \mathbf{E}^2$) and magnetic field energy ($u_H \propto \mu \mathbf{H}^2$) in a cavity due to light's electromagnetic nature, where μ is the permeability [41]; Once giant E-field or H-field hot spots present, this sustaining oscillation is damaged, leading to low-Q resonances.

Second, it has giant radiation loss. In plasmonic cavities, their resonance Q factor reads

$$Q^{-1} = Q_{\mathrm{rad}}^{-1} + Q_{\mathrm{dis}}^{-1}, \tag{1}$$

where Q_{rad} and Q_{dis} are, respectively, the radiation and dissipation Q factors. See SM [18], S1 for simulation and calculation details.

One way to improve the LSPR Q factor is to suppress radiation loss using dark modes with $Q_{\mathrm{rad}} = \infty$. The Q factor for the dark LSPR is $Q \approx 107.8$ at $\alpha = 1.5$ [Fig. 2(a)], representing a 5× improvement over the bright LSPR. This improvement is also attributed to the nonlocality of the dark LSPR. Notably, the resonance wavelength of the dark LSPR ($\lambda_{\mathrm{dark}} \approx 6$ μm) is significantly smaller than that of its bright counterpart ($\lambda_{\mathrm{bright}} \approx 10$ μm). A shorter resonance wavelength enhances nonlocality (see latter discussion and SM [18], S3).

While purely local resonances are limited to isolated plasmonic particles, all resonances in plasmonic arrays exhibit nonlocality due to coupling between neighboring metaunits, resulting in suppressed in-plane radiation (SM [18], S3). In this study, we refer to dark and bright modes in plasmonic arrays with large height scaling parameters (e.g., $\alpha = 1.5$) as local resonances for simplicity, as they are primarily driven by LSPRs. More accurately, these modes should be termed quasi-isolated localized modes.

However, the dark LSPR's Q factor is limited by significant dissipation loss linked to strong local light confinement, observed as hot spots on pillar tops [Fig. 2(d)].

Utilizing our local-to-nonlocal transition strategy effectively minimizes dissipation loss. In this transition, the E field becomes less confined and extends more into the lossless air (SM [18], S4). This is accomplished by increasing mode volumes [Fig. 2(b)] and the gradual disappearance of hot spots on pillar tops, eventually resulting in a uniformly distributed E-field profile on the gold film plane [Fig. 2(d)]. These features substantially reduce resonances' dissipation loss, as indicated by large Q factors, $Q \approx 3439$ (dark) and $Q \approx 3802$ (bright) at $\alpha = 0.01$ for both modes [Fig. 2(a)], several orders of magnitude larger than the local LSPRs. These high-Q nonlocal modes are collective resonances strongly coupled with nonlocal diffraction orders.

Diffraction orders and nonlocality—Collective resonance modes in a plasmonic array can be decomposed into Bloch harmonics [42], given by $\mathbf{E}(\mathbf{r}) = \sum a_{(p,q)} e^{-i(k_\parallel + pG_x + qG_y)\mathbf{r}}$, where $a_{(p,q)}$ is the complex amplitude, $k_\parallel$ the in-plane k vector, $G_x = (2\pi/P_x)\hat{x}$ and $G_y = (2\pi/P_y)\hat{y}$ the array reciprocal vectors, with the metaunit periods $P_x = P_y = P = 3$ μm and $p, q \in \mathbb{Z}$.

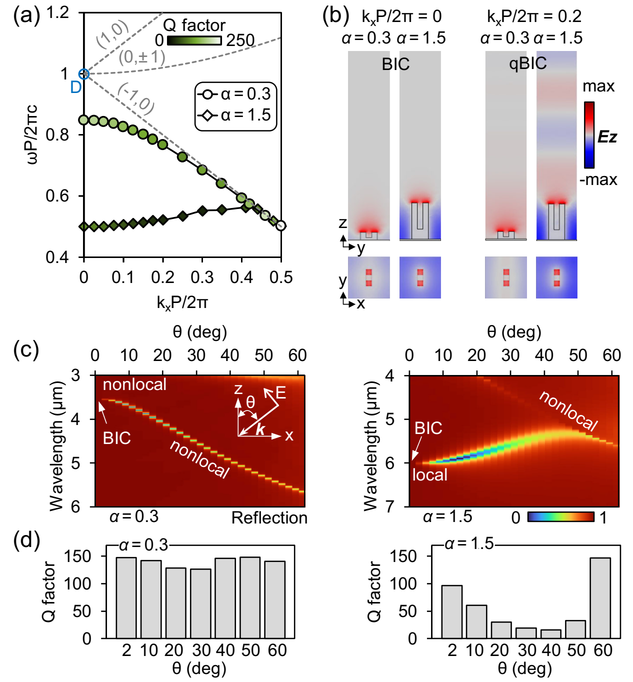

FIG. 3. (a) Calculated band structure for the dark mode with nonlocal ($\alpha = 0.3$) and local ($\alpha = 1.5$) characteristics, denoted by circular and square markers, respectively. The color represents eigenmode Q factor. The gray dashed lines represent three diffraction orders: (1,0), $(-1,0)$, and $(0,\pm1)$. The blue circle denotes the D point. (b) The field distribution of dark modes for two metasurfaces ($\alpha = 0.3$ and $\alpha = 1.5$) at $k_xP/2\pi = 0$ (Γ point) and $k_xP/2\pi = 0.2$ (off Γ). (c) Reflection spectra for two metasurfaces ($\alpha = 0.3$ and $\alpha = 1.5$) at oblique incidence in the x-z plane under TM polarized light excitation (E-field vector in the incident plane). (d) The corresponding Q factor of the two dark modes at different oblique angles. The Q factor is the ratio of resonance wavelength to full width at half maximum.

The empty lattice dispersion equation $|k_\parallel + pG_x + qG_y| = 2\pi/\lambda$ defines momentum space positions where propagating diffraction orders (p, q) emerge [gray dashed lines, Fig. 3(a)]. Specifically, at the Γ point of the array, we identify a highly symmetric position termed the D point [blue circle in Fig. 3(a)], where three diffraction orders (1,0), $(-1,0)$, and $(0,\pm1)$ degenerate. We assign the corresponding operational wavelength $\lambda_D = P$ as the degenerate wavelength.

At Γ-point direction, D point is a critical transition point. Specifically, the Bloch harmonics (1,0), $(-1,0)$, $(0,\pm1)$ can either exist as bounded evanescent waves when $\lambda > \lambda_D$ or transform into propagating diffraction orders when $\lambda < \lambda_D$. At $\lambda = \lambda_D$ those harmonics travel along the array surface at a grazing angle and interact with many metaunits (nonlocality). We use normalized detuning wavelength (Δ) to describe the distance between resonance wavelength λ and λ_D:

$$\Delta = \frac{\lambda - \lambda_D}{\lambda_D} = \frac{\lambda - P}{P}. \tag{2}$$

As Δ decreases approaching zero, LSPRs transition into collective resonances dominated by surface plasmon polaritons (SPPs), (SM [18], S4). LSPRs exhibit strong light confinement (hot spots) and weak interunit coupling. Conversely, SPPs have significantly extended E fields into the air due to strong interaction with nonlocal diffraction orders. This explains the larger mode volumes of nonlocal modes compared to local LSPRs [Fig. 2(b)].

Nonlocal nature of modes—The high-Q nonlocal modes are trapped SPPs, characterized by standing SPP waves confined in a Fabry-Perot cavity (SM [18], S4 and S5). Two pieces of evidence support this interpretation.

First, trapped SPPs exhibit no far-field radiation. Consequently, all nonlocal plasmonic modes, whether transitioning from a dark or bright LSPR in the local to nonlocal shift, should remain subradiative if they are trapped SPPs. The dark LSPR supports this characteristic throughout the transition [Fig. 2(d)]. Interestingly, despite being radiative in local regimes ($\alpha = 1.5$), the bright LSPR becomes less radiative ($\alpha = 0.3$) and eventually becomes radiation-free in nonlocal regimes ($\alpha \leq 0.04$) [see Fig. 2(d) and S4 in SM [18]]. This aligns with the dark feature of trapped SPPs. See S8 in SM [18] for radiation pattern understanding. Second, another evidence is linked to the Q-factor limit of the nonlocal mode.

Q-factor limit—As Δ decreases, dark and bright LSPRs shift into trapped SPPs, exhibiting minimal dissipation loss, enabling efficient energy exchange between E field and H field. To determine the upper limit of Q factors for nonlocal plasmonic resonances, we can assess

$$Q_{\max} = \frac{k_{\mathrm{SPP}}^{r}}{2k_{\mathrm{SPP}}^{i}}, \tag{3}$$

where k_{SPP}^{r} and k_{SPP}^{i} are the real and imaginary part of SPP's k vector, such that $k_{\mathrm{SPP}} = k_{\mathrm{SPP}}^{r} + ik_{\mathrm{SPP}}^{i} = (2\pi/\lambda)\sqrt{[\epsilon\epsilon_0/(\epsilon + \epsilon_0)]}$, where ϵ and ϵ_0 are the permittivities of gold and vacuum [43]. As ϵ varies with wavelength, the maximum Q factor of nonlocal plasmonic resonance is wavelength dependent (SM [18], S6). For $\lambda \approx 3$ μm, the trapped SPP's Q factor is calculated as ~3805, consistent with numerical results of nonlocal mode in Fig. 2(a).

Local-nonlocal transition in the momentum space—The local-to-nonlocal transition can also occur in the momentum space as the resonance modes interact with nonlocal diffraction orders. For example, we calculate the eigenfrequency and Q factor for two dark modes with different height parameters, $\alpha = 1.5$ (local) and $\alpha = 0.3$ (nonlocal); see Fig. 3(a). They are symmetry-protected BICs with zero radiation loss at the Γ point ($k_{\parallel} = 0$); see Fig. 3(b) (left). As the in-plane vector $k_x = (\omega/c)\sin(\theta)$ increases, BICs transit to qBICs with two distinguished properties.

First, the Q factor of the local qBIC mode experiences a rapid decrease, whereas the Q factor of the nonlocal qBIC mode remains stable, as verified by both eigenmode studies

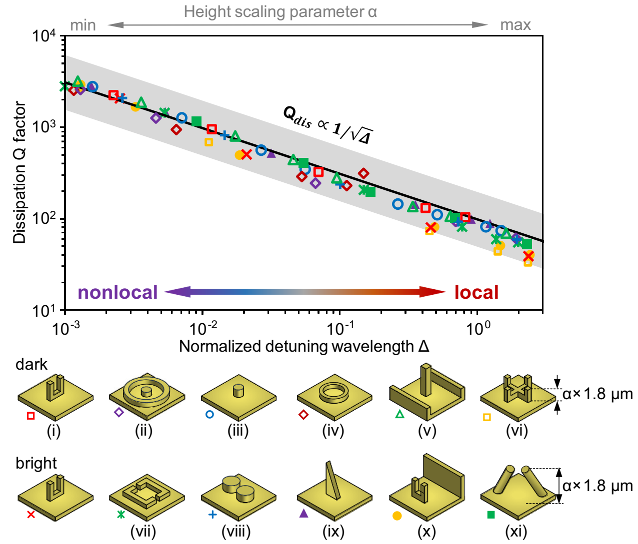

FIG. 4. Dependence of the dissipation Q factor on the normalized detuning wavelength Δ (log-log scale) for various all-plasmonic designs [(i)–(xi)] supports bright and dark LSPRs (Refs. [13–15,44–51]) All square units have a 3 μm period.

[Fig. 3(a)] and full-wave simulations [Figs. 3(c) and 3(d)]. This results from different coupling strengths between the two modes and diffraction order $(-1, 0)$. For example, the resonance frequency of nonlocal mode is closer to diffraction order $(-1, 0)$ than its local counterpart at $k_x P/2\pi = 0.2$. Thus, it relies more on the mutual interaction among neighboring units, which reduces its radiation loss [17]. This makes it less radiative compared to the local counterpart [Fig. 3(b), right]. Also, its nonlocal feature makes it less dissipative. These two features help it keep high-Q resonances at various oblique incidences [Figs. 3(c) and 3(d)].

Second, the local mode becomes nonlocal at large oblique incidence angles ($\theta > 40°$) as it approaches $(-1, 0)$ diffraction order [Fig. 3(c)]. This is evident by a sudden increase in its Q factor when $\theta > 40°$ [Fig. 3(d)].

Local-nonlocal transition in plasmonic metasurfaces—Our approach to improving the Q factor in plasmonic nanostructures by reducing the height parameter is not limited to a specific metasurface with VSRR units. Instead, it is a universally applicable strategy that can be employed for all types of plasmonic metasurfaces with various metaunits, including single pillar, ring, dimmer, triangular prism, pillar wall, and many others [13–15,44–51], as shown in Fig. 4.

All metasurfaces in Fig. 4 support LSPRs. For simplicity, we set them as square units with a 3 μm period and an initial height of 1.8 μm ($\alpha = 1$). They have the same degenerate wavelength $\lambda_D = P = 3$ μm. As the height scaling parameter α decreases, LSPRs (dark or bright) transition into trapped SPPs with similar, symmetric or antisymmetric, E-field profiles (SM [18], S7).

We study the dependence of the dissipation Q factor Q_{dis} on the normalized detuning wavelength Δ for all plasmonic metasurfaces during the local (LSPRs) to nonlocal (trapped SPPs) transition (Fig. 4). An inverse square root law well approximates the relationship,

$$Q_{\mathrm{dis}} \propto \frac{1}{\sqrt{\Delta}}, \tag{4}$$

where Δ is calculated using Eq. (2), and Q_{dis} using Eq. (1) (SM [18], S1). Notably, in pure nonlocal regimes ($\Delta \sim 10^{-3}$), the Q factor ($Q = Q_{\mathrm{dis}}$ as $Q_{\mathrm{rad}} = \infty$) of all plasmonic metasurfaces is approaching ~3800, consistent with prediction using Eq. (3), confirming the trapped SPPs nature of the nonlocal modes.

The inverse square root law suggests an intelligent way to engineer plasmonic structures with on-demand resonance Q factor. Most resonances have hybrid (LSPRs + SPPs) properties during the local-to-nonlocal transition. For example, at $\alpha = 0.3$, the bright mode has both hot spots on pillars' tops (local LSPR feature) and trapped SPPs (nonlocal) on the ground plane [Fig. 2(d)]. Notably, hot spots [52] and high-Q resonances [13] are effective ways to enhance the electromagnetic field. A maximum E-field intensity occurs at some point during this transition (SM [18], S3), which proves beneficial for applications such as nonlinear enhancement [53] and fluorescence enhancement [54].

Equation (4) holds for a broad range, $\Delta \in [10^{-3}, 1]$, allowing diverse Q-factor choices (tens to thousands) for most plasmonic metasurfaces. However, plasmonic Q factors are inherently limited, approaching that of trapped SPPs [Eq. (3)]. Achieving higher Q factors in nonlocal regimes necessitates scaling up the lattice period to extend the operational wavelength, as the maximum Q factor is wavelength dependent. This is shown by $Q_{\mathrm{max}} \sim 627$ at $\lambda = 880$ nm and $Q_{\mathrm{max}} \sim 6330$ at $\lambda = 5$ μm (SM [18], S6). This wavelength-dependent trend aligns with recent experimental results ($Q \sim 80$ in near IR [44] and $Q \sim 500$ in mid-IR [55]).

Conclusion—We have suggested a general conceptual approach for achieving large Q factors in plasmonic metastructures by engineering dissipation Q factor of the resonant modes. Our approach employs an efficient control of local and nonlocal optical response, and it is underpinned by the physics of bound states in the continuum. We believe the suggested strategy may open the door to many novel applications of plasmonic structures including efficient lasing, harmonic generation, biosensing, optical imaging, and entangled photon generation.

Acknowledgments—Y. K. acknowledges useful discussions with A. Bogdanov, O. Martin, M. Petrov, and T. Odom. Y. L. thanks insightful discussion with J. B. Khurgin. This work is supported by National Natural Science Foundation of China (62375232), University Grants Committee/Research Grants Council of the Hong Kong Special Administrative Region, China (Project No. AoE/P-502/20, CRF Projects No. C1015-21E and No. C5031-22G, GRF Projects No. CityU 11300224, No. CityU 15303521 and No. CityU 11305223, and Germany/Hong Kong Joint Research Scheme Project No. G-CityU 101/22), City University of Hong Kong (Projects No. 9380131, No. 9610628, and No. 7005867), the Australian Research Council (Grant No. DP210101292), and the International Technology Center Indo-Pacific (ITC IPAC) via Army Research Office (Contract No. FA520923C0023).

[1] C. W. Hsu, B. Zhen, A. D. Stone, J. D. Joannopoulos, and M. Soljačić, Bound states in the continuum, Nat. Rev. Mater. **1**, 1 (2016).

[2] K. Koshelev, S. Lepeshov, M. Liu, A. Bogdanov, and Y. Kivshar, Asymmetric metasurfaces with high-Q resonances governed by bound states in the continuum, Phys. Rev. Lett. **121**, 193903 (2018).

[3] A. Kodigala, T. Lepetit, Q. Gu, B. Bahari, Y. Fainman, and B. Kanté, Lasing action from photonic bound states in continuum, Nature (London) **541**, 196 (2017).

[4] M.-S. Hwang, H.-C. Lee, K.-H. Kim, K.-Y. Jeong, S.-H. Kwon, K. Koshelev, Y. Kivshar, and H.-G. Park, Ultralow-threshold laser using super-bound states in the continuum, Nat. Commun. **12**, 4135 (2021).

[5] G. Zograf, K. Koshelev, A. Zalogina, V. Korolev, R. Hollinger, D.-Y. Choi, M. Zuerch, C. Spielmann, B. Luther-Davies, D. Kartashov *et al.*, High-harmonic generation from resonant dielectric metasurfaces empowered by bound states in the continuum, ACS Photonics **9**, 567 (2022).

[6] A. Leitis, A. Tittl, M. Liu, B. H. Lee, M. B. Gu, Y. S. Kivshar, and H. Altug, Angle-multiplexed all-dielectric metasurfaces for broadband molecular fingerprint retrieval, Sci. Adv. **5**, eaaw2871 (2019).

[7] F. Yesilkoy, E. R. Arvelo, Y. Jahani, M. Liu, A. Tittl, V. Cevher, Y. Kivshar, and H. Altug, Ultrasensitive hyperspectral imaging and biodetection enabled by dielectric metasurfaces, Nat. Photonics **13**, 390 (2019).

[8] Z. Chen, X. Yin, J. Jin, Z. Zheng, Z. Zhang, F. Wang, L. He, B. Zhen, and C. Peng, Observation of miniaturized bound states in the continuum with ultra-high quality factors, Sci. Bull. **67**, 359 (2022).

[9] J. Jin, X. Yin, L. Ni, M. Soljačić, B. Zhen, and C. Peng, Topologically enabled ultrahigh-Q guided resonances robust to out-of-plane scattering, Nature (London) **574**, 501 (2019).

[10] S. I. Azzam, V. M. Shalaev, A. Boltasseva, and A. V. Kildishev, Formation of bound states in the continuum in hybrid plasmonic-photonic systems, Phys. Rev. Lett. **121**, 253901 (2018).

[11] Z. Wang, Y. Liang, J. Qu, M. K. Chen, M. Cui, Z. Cheng, J. Zhang, J. Yao, S. Chen, D. P. Tsai *et al.*, Plasmonic bound states in the continuum for unpolarized weak spatially coherent light, Photonics Res. **11**, 260 (2023).

[12] A. Lovera, B. Gallinet, P. Nordlander, and O. J. Martin, Mechanisms of Fano resonances in coupled plasmonic systems, ACS Nano **7**, 4527 (2013).

[13] Y. Liang, K. Koshelev, F. Zhang, H. Lin, S. Lin, J. Wu, B. Jia, and Y. Kivshar, Bound states in the continuum in anisotropic plasmonic metasurfaces, Nano Lett. **20**, 6351 (2020).

[14] Y. Liang, H. Lin, S. Lin, J. Wu, W. Li, F. Meng, Y. Yang, X. Huang, B. Jia, and Y. Kivshar, Hybrid anisotropic plasmonic metasurfaces with multiple resonances of focused light beams, Nano Lett. **21**, 8917 (2021).

[15] A. Aigner, A. Tittl, J. Wang, T. Weber, Y. Kivshar, S. A. Maier, and H. Ren, Plasmonic bound states in the continuum to tailor light-matter coupling, Sci. Adv. **8**, eadd4816 (2022).

[16] K. L. Koshelev, Z. F. Sadrieva, A. A. Shcherbakov, Y. S. Kivshar, and A. A. Bogdanov, Bound states of the continuum in photonic structures, Phys. Usp. **66**, 494 (2023).

[17] V. G. Kravets, A. V. Kabashin, W. L. Barnes, and A. N. Grigorenko, Plasmonic surface lattice resonances: A review of properties and applications, Chem. Rev. **118**, 5912 (2018).

[18] See Supplemental Material at http://link.aps.org/supplemental/10.1103/PhysRevLett.133.053801 for simulation details, mode volume calculation, single particle resonances vs array resonances, dissipation loss control during the transition between local and nonlocal regimes, trapped SPPs, dissipation Q-factor limit of trapped SPPs, and local and nonlocal transition for various plasmonic metasurfaces, which includes Refs. [19–40].

[19] R. L. Olmon, B. Slovick, T. W. Johnson, D. Shelton, S.-H. Oh, G. D. Boreman, and M. B. Raschke, Optical dielectric function of gold, Phys. Rev. B **86**, 235147 (2012).

[20] S. A. Maier, Plasmonic field enhancement and SERS in the effective mode volume picture, Opt. Express **14**, 1957 (2006).

[21] J. R. Krenn, A. Dereux, J.-C. Weeber, E. Bourillot, Y. Lacroute, J.-P. Goudonnet, G. Schider, W. Gotschy, A. Leitner, F. R. Aussenegg *et al.*, Squeezing the optical near-field zone by plasmon coupling of metallic nanoparticles, Phys. Rev. Lett. **82**, 2590 (1999).

[22] R. W. Wood, XlII. On a remarkable case of uneven distribution of light in a diffraction grating spectrum, London, Edinburgh, Dublin Philos. Mag. J. Sci. **4**, 396 (1902).

[23] W. Zhou and T. W. Odom, Tunable subradiant lattice plasmons by out-of-plane dipolar interactions, Nat. Nanotechnol. **6**, 423 (2011).

[24] P. Zijlstra, P. M. Paulo, and M. Orrit, Optical detection of single non-absorbing molecules using the surface plasmon resonance of a gold nanorod, Nat. Nanotechnol. **7**, 379 (2012).

[25] N. Liu, M. Mesch, T. Weiss, M. Hentschel, and H. Giessen, Infrared perfect absorber and its application as plasmonic sensor, Nano Lett. **10**, 2342 (2010).

[26] M. S. Bin-Alam, O. Reshef, Y. Mamchur, M. Z. Alam, G. Carlow, J. Upham, B. T. Sullivan, J.-M. Ménard, M. J. Huttunen, R. W. Boyd *et al.*, Ultra-high-Q resonances in plasmonic metasurfaces, Nat. Commun. **12**, 974 (2021).

[27] X. Yu, L. Shi, D. Han, J. Zi, and P. V. Braun, High quality factor metallodielectric hybrid plasmonic-photonic crystals, Adv. Funct. Mater. **20**, 1910 (2010).

[28] R. W. Wood, Anomalous diffraction gratings, Phys. Rev. **48**, 928 (1935).

[29] J. T. Y. Tse and H. C. Ong, Quality factor of plasmonic monopartite and bipartite surface lattice resonances, Phys. Rev. B **104**, 125442 (2021).

[30] A. Sobhani, A. Manjavacas, Y. Cao, M. J. McClain, F. J. García de Abajo, P. Nordlander, and N. J. Halas, Pronounced linewidth narrowing of an aluminum nanoparticle plasmon resonance by interaction with an aluminum metallic film, Nano Lett. **15**, 6946 (2015).

[31] S. Zhang, D. A. Genov, Y. Wang, M. Liu, and X. Zhang, Plasmon-induced transparency in metamaterials, Phys. Rev. Lett. **101**, 047401 (2008).

[32] Z. Wang, Y. Wang, Z. Cheng, J. Qu, M. Cui, D. Huang, and C. Yu, Tunable flatband plasmonic quasi-bound states in the continuum based on graphene-assisted metasurfaces, Appl. Phys. Lett. **123**, 121703 (2023).

[33] H. J. Huang, C. P. Yu, H. C. Chang, K. P. Chiu, H. M. Chen, R. S. Liu, and D. P. Tsai, Plasmonic optical properties of a single gold nano-rod, Opt. Express **15**, 7132 (2007).

[34] W.-Y. Tsai, T. L. Chung, H.-H. Hsiao, J.-W. Chen, R. J. Lin, P. C. Wu, G. Sun, C.-M. Wang, H. Misawa, and D. P. Tsai, Second harmonic light manipulation with vertical split ring resonators, Adv. Mater. **31**, 1806479 (2019).

[35] L. F. Tadesse, C.-S. Ho, D.-H. Chen, H. Arami, N. Banaei, S. S. Gambhir, S. S. Jeffrey, A. A. Saleh, and J. Dionne, Plasmonic and electrostatic interactions enable uniformly enhanced liquid bacterial surface-enhanced raman scattering (SERS), Nano Lett. **20**, 7655 (2020).

[36] E. A. Coronado and G. C. Schatz, Surface plasmon broadening for arbitrary shape nanoparticles: A geometrical probability approach, J. Chem. Phys. **119**, 3926 (2003).

[37] A. Wiener, A. I. Fernández-Domínguez, A. P. Horsfield, J. B. Pendry, and S. A. Maier, Nonlocal effects in the nanofocusing performance of plasmonic tips, Nano Lett. **12**, 3308 (2012).

[38] Y. Yang, I. I. Kravchenko, D. P. Briggs, and J. Valentine, All-dielectric metasurface analogue of electromagnetically induced transparency, Nat. Commun. **5**, 5753 (2014).

[39] N. Liu, L. Langguth, T. Weiss, J. Kästel, M. Fleischhauer, T. Pfau, and H. Giessen, Plasmonic analogue of electromagnetically induced transparency at the Drude damping limit, Nat. Mater. **8**, 758 (2009).

[40] B. Gallinet, T. Siegfried, H. Sigg, P. Nordlander, and O. J. Martin, Plasmonic radiance: Probing structure at the angstrom scale with visible light, Nano Lett. **13**, 497 (2013).

[41] J. B. Khurgin, How to deal with the loss in plasmonics and metamaterials, Nat. Nanotechnol. **10**, 2 (2015).

[42] R. J. P. Engelen, D. Mori, T. Baba, and L. Kuipers, Subwavelength structure of the evanescent field of an optical Bloch wave, Phys. Rev. Lett. **102**, 023902 (2009).

[43] A. V. Zayats, I. I. Smolyaninov, and A. A. Maradudin, Nano-optics of surface plasmon polaritons, Phys. Rep. **408**, 131 (2005).

[44] A. Yang, Z. Li, M. P. Knudson, A. J. Hryn, W. Wang, K. Aydin, and T. W. Odom, Unidirectional lasing from template-stripped two-dimensional plasmonic crystals, ACS Nano **9**, 11582 (2015).

[45] A. E. Cetin and H. Altug, Fano resonant ring/disk plasmonic nanocavities on conducting substrates for advanced biosensing, ACS Nano **6**, 9989 (2012).

[46] B. Gerislioglu, L. Dong, A. Ahmadivand, H. Hu, P. Nordlander, and N. J. Halas, Monolithic metal dimer-on-film structure: New plasmonic properties introduced by the underlying metal, Nano Lett. **20**, 2087 (2020).

[47] Z. Li, S. Butun, and K. Aydin, Ultranarrow band absorbers based on surface lattice resonances in nanostructured metal surfaces, ACS Nano **8**, 8242 (2014).

[48] Z. Shen, X. Fang, S. Li, W. Yin, L. Zhang, and X. Chen, Terahertz spin-selective perfect absorption enabled by quasi-bound states in the continuum, Opt. Lett. **47**, 505 (2022).

[49] Y. Tang, Y. Liang, J. Yao, M. K. Chen, S. Lin, Z. Wang, J. Zhang, X. G. Huang, C. Yu, and D. P. Tsai, Chiral bound states in the continuum in plasmonic metasurfaces, Laser Photonics Rev. **17**, 2200597 (2023).

[50] X. Xiong, S.-C. Jiang, Y.-H. Hu, R.-W. Peng, and M. Wang, Structured metal film as a perfect absorber, Adv. Mater. **25**, 3994 (2013).

[51] P. Zilio, M. Malerba, A. Toma, R. P. Zaccaria, A. Jacassi, and F. D. Angelis, Hybridization in three dimensions: A novel route toward plasmonic metamolecules, Nano Lett. **15**, 5200 (2015).

[52] D. P. Tsai, J. Kovacs, Z. Wang, M. Moskovits, V. M. Shalaev, J. S. Suh, and R. Botet, Photon scanning tunneling microscopy images of optical excitations of fractal metal colloid clusters, Phys. Rev. Lett. **72**, 4149 (1994).

[53] R. Czaplicki, A. Kiviniemi, M. J. Huttunen, X. Zang, T. Stolt, I. Vartiainen, J. Butet, M. Kuittinen, O. J. Martin, and M. Kauranen, Less is more: Enhancement of second-harmonic generation from metasurfaces by reduced nanoparticle density, Nano Lett. **18**, 7709 (2018).

[54] K. A. Sergeeva, D. V. Pavlov, A. A. Seredin, E. V. Mitsai, A. A. Sergeev, E. B. Modin, A. V. Sokolova, T. C. Lau, K. V. Baryshnikova, M. I. Petrov *et al.*, Laser-printed plasmonic metasurface supporting bound states in the continuum enhances and shapes infrared spontaneous emission of coupled HgTe quantum dots, Adv. Funct. Mater. **33**, 2307660 (2023).

[55] S.-Q. Li, W. Zhou, D. Bruce Buchholz, J. B. Ketterson, L. E. Ocola, K. Sakoda, and R. P. Chang, Ultra-sharp plasmonic resonances from monopole optical nanoantenna phased arrays, Appl. Phys. Lett. **104** (2014).